



Static Magnetic Properties of Cryogel® and Pyrogel® at Low Temperatures and in High Magnetic Fields

Caeli L. Benyacko^{1,5} · Garrett T. Hauser^{1,6} · Raven J. Rawson¹ · Alan J. Sherman¹ · Quinton L. Wiebe¹ · Krittin Poottafai³ · Daniel R. Talham³ · Mark W. Meisel^{1,2,4}

Received: 14 April 2025 / Accepted: 17 June 2025

© The Author(s), under exclusive licence to Springer Science+Business Media, LLC, part of Springer Nature 2025

Abstract

The static magnetic properties of the silica-based aerogels of Cryogel® and Pyrogel®, manufactured by Aspen Aerogels®, were measured over a range of temperatures ($2\text{ K} \leq T \leq 400\text{ K}$) and in magnetic fields up to 70 kG. These data and a model of the responses are reported, so these properties are familiar to others who may benefit from knowing them before the materials are employed in potential applications.

Keywords Aerogels · Magnetic properties · Low temperatures · High magnetic fields

1 Motivation

Using the phrase “low-temperature aerogels” during a search for thermal isolation materials, a paper by a CERN-based research team appeared [1], which reported studies of the thermal conductivity of Cryogel®, but the magnetic properties were not found in any database. While learning more about the low-temperature insulation trademarked as Cryogel® by Aspen Aerogels [2], the high-temperature counterpart Pyrogel® was identified as potential insulation for a materials processing in high magnetic fields station that was being constructed [3, 4]. Consequently, a sample pack was purchased, and undergraduate research students were trained to acquire, analyze, and report the magnetic data [5–7].

In an attempt to be useful to others who may be interested in the low temperature and high magnetic field results, this brief report summarizes the findings and discusses the outcomes with a focus on Cryogel®, while the magnetic properties of Pyrogel® are also presented. After overviewing the samples and methods employed, the low-field temperature dependences and isothermal responses of the magnetism are presented, analyzed, and summarized.

Extended author information available on the last page of the article

Table 1 Compositions of Cryogel® and Pyrogel® reported in this work

Constituent	Formula	Composition (%)		
		Cryogel® X201 [8]	Cryogel® Z [9]	Pyrogel® XTE [10]
Synthetic Amorphous Silica	SiO ₂	40–50	25–40	30–40
Methylsilylated Silica	C ₆ H ₁₉ NSi ₂	10–20	10–20	10–20
Polyethylene Terephthalate	C ₁₀ H ₈ O ₄	10–20	10–20	
Fibrous Glass (textile grade) ^a	SiO ₂	10–20	10–20	40–50
Magnesium Hydroxide	Mg(OH) ₂	0–5	0–5	
Aluminum Foil ^b	Al		0–5	
Iron Oxide (Fe(III) oxide)	Fe ₂ O ₃			1–10
Aluminum Trihydrate	AlH ₃ O ₃			1–5

The exact percentages (concentrations) of the compositions were withheld as trade secrets

^aThe Chemical Abstracts Service Registry Number was not given, so our assumption is listed here

^bSamples were taken in regions away from this foil and its immediate region

2 Samples and Methods

The sample pack received contained nominally (40 cm)² sheets of five materials; specifically, the samples (and their thicknesses) were: Cryogel®X201 (5 and 10 mm) [8], Cryogel®Z (5 and 10 mm) [9], and Pyrogel®XTE (10 mm) [10], whose compositions are provided in Table 1. During the course of the study, two different sections of each sheet were used to harvest samples, and at least two samples from each section were studied over the course of the study.

Samples, with a typical mass, m , in the range 20–40 mg, were extracted from the sheets and gently pressed directly into a ~ 7 -mm-long section of the straw sample holders, which provided a uniform background for the detection scheme used by the commercial magnetometer, Quantum Design MPMS XL, capable of providing a range of temperature ($2\text{ K} \leq T \leq 400\text{ K}$) and magnetic field ($-70\text{ kG} \leq B \leq 70\text{ kG}$) conditions. When studying Cryogel®Z, the aerogel-like samples were taken from a region away from the aluminum foil and its immediate surrounding location. The studies of the temperature dependence of the low-field magnetization were performed in zero field cooling (ZFC) and field cooling (FC) modes and were then followed by isothermal (usually at $T = 5\text{ K}$) magnetization measurements while increasing ($B = 0 \rightarrow 70\text{ kG}$) and then decreasing ($B = 70\text{ kG} \rightarrow -10\text{ kG}$) the field to check for hysteresis. For this report, the data are expressed in cgs units where a magnetic moment, μ , is $1\text{ emu} = 1\text{ erg G}^{-1}$ [11], so the following notation is employed for the mass magnetization $M = \mu/m$ (emu/g) and the mass susceptibility $\chi = M/B$ (emu g⁻¹ G⁻¹).

At an early stage in the project, the ability to establish the mass of a sample being studied was recognized as an issue because sample handling caused shards to be shed from the bundles that were prepared. In some instances, fibers were

detected in the lower end of the straw holders, as described in the following section, where the results of specific samples are presented and framed in the context of the overall reproducibility of the magnetic response reported herein.

For inductively coupled plasma optical-emission spectroscopy (ICP-OES), a Pyrogel®XTE or Cryogel®X201 sample with a mass of 10 mg was dissolved in 20 mL of 1 M KOH solution and left overnight to allow the silica to be digested so the metal ions could dissociate from the fiber. The solution was then adjusted to an acidic pH using 1 M HNO₃ to dissolve any metal oxide and subsequently diluted with deionized water to make the final sample solution. The ICP-OES study employed a VARIAN VISTA RL simultaneous spectrometer (Agilent Technologies, Santa Clara, California, USA) using standard addition methods. These spectroscopic analyses were performed as simple verifications of our hypotheses about the possible sources of the magnetic responses observed, and a complete characterization of each sample sheet is beyond the scope of work for this project.

3 Magnetic Data and Discussion

In low applied magnetic fields, the initial conjecture was the high-temperature magnetic signal that would be dominated by the diamagnetism of the SiO₂ matrix [12], and the low-temperature response might show evidence of some trace amounts of free-spin $S = 1/2$ impurities [13, 14] for Cryogel®, whereas signatures reminiscent of the well-studied magnetism of Fe(III)₂O₃ [15] were anticipated for Pyrogel®.

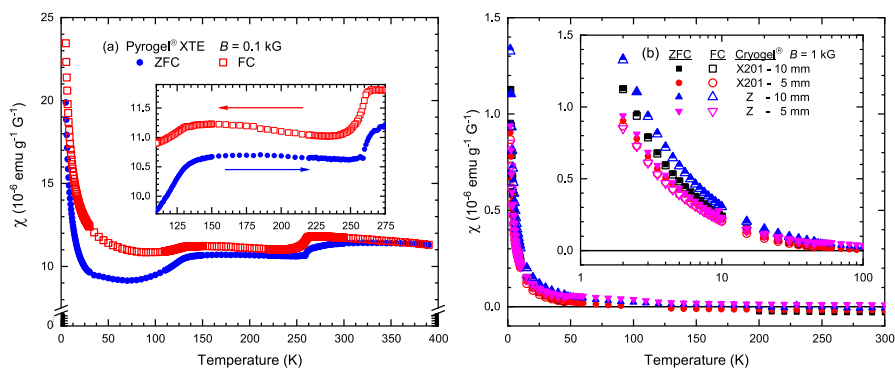


Fig. 1 The temperature-dependent magnetic susceptibilities of Pyrogel®XTE and the 5- and 10-mm-thick sheets of Cryogel®X201 and Cryogel®Z are shown. **a** The mass susceptibility of Pyrogel®XTE measured in $B = 0.1$ kG exhibits a strong Curie-like tail at low temperatures, differences between FC and ZFC data below a blocking temperature near 130 K, and a sharp shoulder at the Morin transition of 260 K, which are assignable to the known presence of Fe₂O₃, see Table 1. **b** The low magnetic field ($B = 1$ kG) mass susceptibility data for all four samples of Cryogel® are almost degenerate on a linear temperature scale, so the inset shows the results on a logarithmic scale for $T < 100$ K. In most instances, the ZFC and FC data are the same within measuring uncertainty, and the strength of the Curie-like response at low temperature is striking

Although some of these signatures appeared in the data, Fig. 1, other features were not anticipated.

More specifically for Pyrogel®XTE, Fig. 1a, the differences between ZFC and FC traces below a blocking temperature of ≈ 130 K and a strong Curie-like tail were not surprising [16], while the appearance of the magnetic “fingerprints” of a Morin transition at 260 K [17–19] was not anticipated. Since Fe(III) oxide is listed as an ingredient of Pyrogel®, see Table 1, the observed magnetic behavior is consistent with the presence of a broad distribution of Fe_2O_3 nanoparticles with diameters in the range of 10–100 nm [18, 19].

In contrast to Pyrogel®, the high-temperature magnetic responses of Cryogel® are dominated by the diamagnetic signal, which is eventually overcome by a paramagnetic contribution as the temperature is lowered, Fig. 1b. Consequently, some gaps in the data sets appear as the signal changes sign passing through zero when nearly equal amounts of diamagnetic and paramagnetic signals are present.

A striking aspect of the magnetism of the Cryogel® samples is the strong strength of the Curie-like tail below nominally 50 K, Fig. 1b. Since all of the data appear to be almost degenerate on a linear temperature scale, the inset shows an expanded view of the data on a logarithmic scale where essentially any differences between the ZFC and FC data are within the experimental resolution. Subtle differences between the four samples are noticeable and were also detected in the low-temperature isothermal magnetization studies, as shown in the inset of Fig. 2a. In fact, these results capture a major issue of establishing the mass of the sample being studied. Extracting samples from the sheets involved cutting the materials in various ways, and all methods led to the samples shedding small shards of their contents when being handled, with some material detected in the tape-end-cap at the bottom of the straw used for the magnetometry studies. Consequently, these data were normalized to their $M(70 \text{ kG}, 5 \text{ K})$ values, see Table 2, and with the exception of the results for Cryogel®X201—5 mm, a

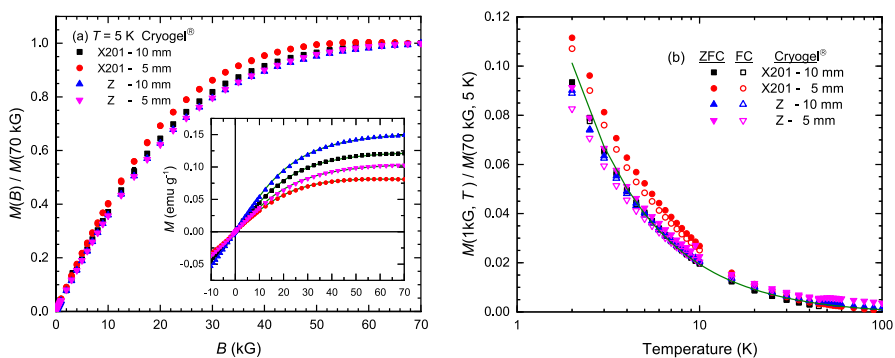


Fig. 2 **a** The magnetic field dependences of the isothermal magnetic moments, $M(B, 5 \text{ K})$ of Cryogel®, are shown per gram of sample in the inset and in dimensionless form when normalized to their $M(70 \text{ kG}, 5 \text{ K})$ values. **b** The data from Fig. 1b inset are replotted in dimensionless form. The green lines for the inset of (a) and for (b) represent the results of the model, see text and parameters in Table 2. For clarity, the X201—10 mm result is shown in (b)

Table 2 Details of samples measured and parameters providing phenomenological approximations of the magnetic responses

Sample	File ID	Mass (mg)	$M(70 \text{ kG}, 5 \text{ K})^a$ (emu g ⁻¹)	χ_o (10 ⁻⁶ emu g ⁻¹ G ⁻¹)
Cryogel®X201—10 mm	230206	28.96	0.1210	− 1.0
Cryogel®X201—5 mm	230126	27.18	0.0811	− 2.5
Cryogel®Z—10 mm	230201	29.77	0.1491	− 0.5
Cryogel®Z—5 mm	230214	35.72	0.1029	− 0.5
Pryogel®XTE—S1 ^b	220623	22.02	NA	—
Pryogel®XTE—S2 ^b	220701	24.23	0.4112	+ 1.0

^aThe overall uncertainty of these values is less than $\pm 3\%$

^bTwo different samples, S1 for Fig. 1a and S2 for Fig. 3

universal trend is established within the experimental uncertainty of the magnetic signals, Fig. 2a. To further clarify this issue, the data in the inset of Fig. 1b were normalized to their $M(70 \text{ kG}, 5 \text{ K})$ values, Fig. 2b, which also provides a sense of the magnetic response independent of the mass of the sample.

The isothermal magnetization of Pyrogel®XTE is shown in Fig. 3, where up/down refers to the field sweeping up/down. At 300 K, the first measurement was taken immediately after inserting the sample into the magnetometer, and the second run was made after the sample was “degassed” while measuring in 0.1 kG from 300 to 390 K over a period of 4 h before cooling the sample back to 300 K. During the heating cycle, the magnetic signal subtly decreased for the first 90 min and was then independent of the conditions. Although the initial parts of each $M(B, 300 \text{ K})$ run are slightly history dependent, the return to zero field conditions indicates no substantial impact of the magnetic response due to the heating cycle, see Fig. 3b. Two different studies were also conducted at 5 K to check

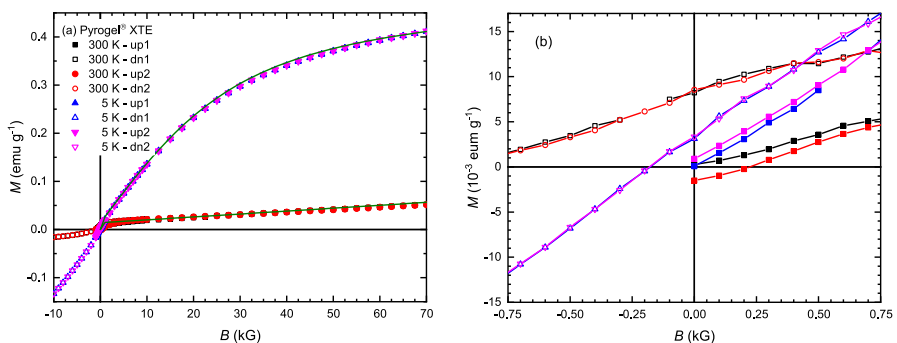


Fig. 3 The magnetic field dependences of the isothermal magnetic moments, $M(B, 5 \text{ and } 300 \text{ K})$ of Pyrogel®XTE are shown in **a** for up and down (dn) sweeps as described in the text and with the modeling results shown by solids lines and in **b** as an expanded view in the region near the origin and where the lines connect the data points

reproducibility and history dependences of the sample, and the overall magnetic response was determined to be robust, Fig. 3.

Lastly, since the low-field plots of Figs. 1b and 2b do not elucidate subtle trends that may exist in the region of the strong Curie-like tail, the mass-independent normalized data of Fig. 2b were used to generate the effective $\chi \times T$ versus T plot of Fig. 4, where additional fidelity is revealed. For the instrument being used, the cooling mechanism employed switches below 4.5 K, resulting in additional time to cool samples to the minimum temperature. Consequently, as is the case in these data sets, the $T = 2$ K data point possesses evidence of not being in thermal equilibrium before the measurement was performed. From this viewpoint, the $T \lesssim 10$ K data, acquired over a period of 1 h after stabilizing at $T = 2$ K, may have been acquired when the sample was not in thermal equilibrium with the thermometer of the instrument. However, the isothermal magnetization studies performed at 5 K (chosen to avoid concerns about thermal equilibrium) take nominally 5 h to complete but do not show any hysteresis that would arise from non-equilibrium conditions.

Taken ensemble, the results motivated a check of the level of magnetic species that might be present in the samples, an ICP-OES study was performed. With no other metal being detected, Fe was detected at 0.26%w/w for Pyrogel®XTE and at 0.09%w/w for Cryogel®X201. These values are considered as lower bounds due to the incomplete dissociation of the silica in the samples. The Fe content levels were not explored in greater detail since this thrust was beyond the scope of this work.

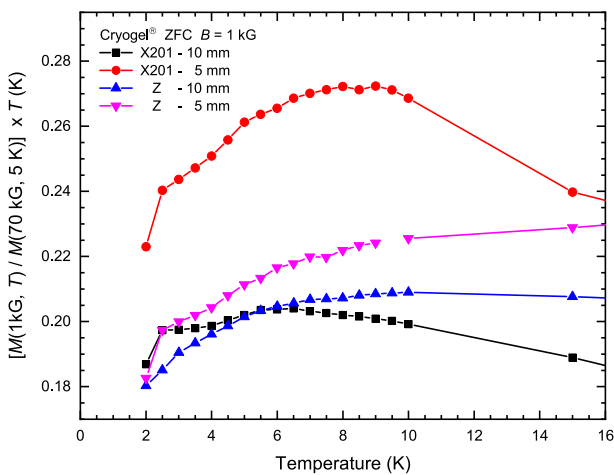


Fig. 4 The normalized, $B = 1$ kG data for Cryogel® shown in Fig. 2b are multiplied by temperature and are replotted on a linear scale below 15 K. The solid lines connect neighboring data points, and the inferences are discussed in the text

4 Phenomenological Model

At the start of this work, the goal was to characterize the magnetism of Cryogel® arising from conjectured trace amounts of non-interacting species, with total angular momentum J and g -factor values, which might be described the Brillouin function, $\mathcal{B}_J(J, g, B, T)$ [11]. Specifically for a sample of mass m and with N entities, the predicted mass magnetization can be written as

$$M(B, T) = \frac{N}{m} J g \mu_B \mathcal{B}_J(g, J, B, T), \quad (1)$$

where μ_B is the Bohr magneton. Given the difficulty in establishing the mass of the samples, each side Eq. (1) can be normalized by the measured $M(70 \text{ kG}, 5 \text{ K})$ values for each sample to yield

$$\frac{M(B, T)}{M(70 \text{ kG}, 5 \text{ K})} = \frac{\mathcal{B}_J(g, J, B, T)}{\mathcal{B}_J(g, J, 70 \text{ kG}, 5 \text{ K})} + \frac{\chi_o B}{\mathcal{B}_J(g, J, 70 \text{ kG}, 5 \text{ K})}, \quad (2)$$

where a temperature-independent term is added to accommodate the diamagnetism from the silica. Equation (2) provides motivation for generating Fig. 2 and also yields the green lines when using the values listed in Table 2 with $J = 5/2$ and $g = 2.03$ [20, 21].

With respect to the results for Pyrogel®XTE, there is no basis for a non-interacting spin model to be valid. Nonetheless, Eq. (2) provides the green lines shown in Fig. 3a when using the values listed in Table 2 with $J = 5/2$ and $g = 2$ [20, 21], albeit with the accommodation of a constant 0.014 emu g^{-1} remanent magnetization, Fig. 3b.

5 Summary

By providing a survey of the static magnetic properties of Cryogel® and Pyrogel®XTE at low temperatures and in high magnetic fields, this brief report fills a void in the literature about these properties which need to be known before deployment in some potential applications. A phenomenological model provides reasonable estimates for the magnetism observed, but of course, the specific outcomes are likely to be fabrication batch dependent on an industrial scale, and this reason may explain the X201—5 mm results being different than the responses detected from the other Cryogel® materials.

Acknowledgements The National Science Foundation (NSF) Research Experiences for Undergraduates (REU) funding provided support for the participation of: QLW and AJS (Fall 2021 and Spring 2022) and CLB (Spring 2022) via DMR-1708410; GTH and RJR (Summer 2022) and CLB (Fall 2022) via MagLab REU Program DMR-1644779; CLB (Summer 2022) via UF Condensed Matter and Applied Materials REU Program DMR-1852138, which also provided professional development and social networking activities to GTH and RJR (Summer 2022); and CLB (Spring 2023, Fall 2023, and Spring 2024) via MagLab DMR-2128556. The University of Florida University Scholars Program (USP) and Center for Undergraduate Research (CUR) provided additional support to CLB (Fall 2023 and Spring 2024).

Aspects of this work also used facilities and personnel supported by the National High Magnetic Field Laboratory (NHMFL or MagLab), via NSF Cooperative Agreement DMR-1644779 and DMR-2128556, and the State of Florida. Patience on the part of all stakeholders is gratefully acknowledged as this work was initiated during the pandemic.

Author Contributions C.L.B., G.T.H., R.J.R., A.J.S., Q.L.W., and M.W.M. collected, plotted, and analyzed magnetic data. K.P. and D.R.T. collected and analyzed the spectroscopic data. C.L.B. and M.W.M. drafted the manuscript. C.L.B., G.T.H., K.P., D.R.T., and M.W.M. contributed to the final version of the manuscript.

Data Availability The magnetic response data presented herein are publicly available as cvs-files on the Open Science Framework (OSF) repository [22].

Declarations

Conflict of interest The authors declare no competing interests.

References




1. V. Ilardi, L.N. Busch, A. Dudarev, T. Koettig, P. Borges de Sousa, J. Liberadzka, H. Silva, H. Kate, Compression and thermal conductivity tests of Cryogel@z for use in the ultra-transparent cryostats of FCC detector solenoids. *IOP Conf. Ser. Mater. Sci. Eng.* **756**(1), 012005 (2020). <https://doi.org/10.1088/1757-899X/756/1/012005>
2. Aspen Aerogels: Products (2025), <https://www.aerogel.com/>. Accessed 20 March 2025
3. S. Flynn, M.E. Bates, J.C. Lee, M.R. Tonks, M.S. Kesler, M.V. Manuel, V.M. Miller, M.W. Meisel, J.J. Hamlin, A simultaneous high temperature and high magnetic field furnace for advanced materials synthesis and processing. *Bull. Am. Phys. Soc.* **MAR22**, K31.9 (2022). <https://meetings.aps.org/Meeting/MAR22/Session/K31.9>
4. S. Flynn, C.L. Benyacko, M. Mihalik, J. Lee, F. Ma, M.E. Bates, S. Sinha, K.A. Abboud, M. Mihalik, M.W. Meisel, J.J. Hamlin, Synthesis of cobalt grown from Co-S eutectic in high magnetic fields (2025). <https://arxiv.org/abs/2504.00788>
5. A.J. Sherman, Q.L. Wiebe, M.W. Meisel, An experimental study of the magnetic properties of Cryogel. *Bull. Am. Phys. Soc.* **MAR22**, A47.14 (2022). <https://meetings.aps.org/Meeting/MAR22/Session/A47.14>
6. Q.L. Wiebe, A.J. Sherman, M.W. Meisel, Characterization of the magnetic properties of Pyrogel. *Bull. Am. Phys. Soc.* **MAR22**, A47.15 (2022). <https://meetings.aps.org/Meeting/MAR22/Session/A47.15>
7. C.L. Benyacko, A.J. Sherman, R.J. Rawson, Q.L. Wiebe, G.T. Hauser, K. Poottaifai, D.R. Talham, M.W. Meisel, Characterization of the low temperature static magnetic properties of Cyrogel. *Bull. Am. Phys. Soc.* **MAR24**, S12.6 (2024). <https://meetings.aps.org/Meeting/MAR24/Session/S12.6>
8. Aspen Aerogels: Safety Data Sheet. Aspen Aerogels (2015), <https://www.pacorinc.com/aerogel-insulation>. Accessed 4 Nov 2021
9. Aspen Aerogels: Safety Data Sheet. Aspen Aerogels (2015), <https://www.pacorinc.com/aerogel-insulation/>. Accessed 4 Nov 2021
10. Aspen Aerogels: Safety Data Sheet. Aspen Aerogels (2017), <https://www.pacorinc.com/aerogel-insulation/>. Accessed 4 Nov 2021
11. S. Blundell, *Magnetism in Condensed Matter* (Oxford University Press, Oxford, 2001), pp.194–196. <https://doi.org/10.1093/oso/9780198505921.001.0001>
12. *CRC Handbook of Chemistry and Physics*. CRC Press, Boca Raton, FL. Online version: Section of *Magnetic Susceptibility of Selected Inorganic Compounds*, Row 379 (2024). <https://www.routledge.com/CRC-Handbook-of-Chemistry-and-Physics/Rumble/p/book/9781032655628>
13. M.P. Sarachik, F. Michelman, W. Li, F.W. Smith, J.P. Remeika, Magnetic study of carbon chars in the transition range. *J. Appl. Phys.* **58**(7), 2681–2685 (1985). <https://doi.org/10.1063/1.335903>, https://pubs.aip.org/aip/jap/article-pdf/58/7/2681/18413103/2681_1_online.pdf

14. T. Matsuoka, L.S. Vlasenko, M.P. Vlasenko, T. Sekiguchi, K.M. Itoh, Identification of a paramagnetic recombination center in silicon/silicon-dioxide interface. *Appl. Phys. Lett.* **100**(15), 152107 (2012). <https://doi.org/10.1063/1.3702785>, https://pubs.aip.org/aip/apl/article-pdf/doi/10.1063/1.3702785/13019107/152107_1_online.pdf
15. R. Zboril, M. Mashlan, D. Petridis, Iron(III) oxides from thermal process synthesis, structural and magnetic properties, Mössbauer spectroscopy characterization, and applications. *Chem. Mater.* **14**(3), 969–982 (2002). <https://doi.org/10.1021/cm0111074>
16. L. Maldonado-Camargo, M. Unni, C. Rinaldi, in *Magnetic Characterization of Iron Oxide Nanoparticles for Biomedical Applications*, ed. by S.H. Petrosko, E.S. Day (Springer, New York, 2017), pp.47–71. https://doi.org/10.1007/978-1-4939-6840-4_4
17. F.J. Morin, Magnetic susceptibility of $\alpha\text{-Fe}_2\text{O}_3$ and $\alpha\text{-Fe}_2\text{O}_3$ with added titanium. *Phys. Rev.* **78**, 819–820 (1950). <https://doi.org/10.1103/PhysRev.78.819.2>
18. L. Suber, A.G. Santiago, D. Fiorani, P. Imperatori, A.M. Testa, M. Angiolini, A. Montone, J.L. Dormann, Structural and magnetic properties of $\alpha\text{-Fe}_2\text{O}_3$ nanoparticles. *Appl. Organomet. Chem.* **12**(5), 347–351 (1998). [https://doi.org/10.1002/\(SICI\)1099-0739\(199805\)12:5<347::AID-AOC729>3.0.CO;2-G](https://doi.org/10.1002/(SICI)1099-0739(199805)12:5<347::AID-AOC729>3.0.CO;2-G)
19. D. Kubániová, L. Kubíčková, T. Kmječ, K. Závěta, D. Nižňanský, P. Brázda, M. Klementová, J. Kohout, Hematite: Morin temperature of nanoparticles with different size. *J. Magn. Magn. Mater.* **475**, 611–619 (2019). <https://doi.org/10.1016/j.jmmm.2018.11.126>
20. D. Goldfarb, M. Bernardo, K.G. Strohmaier, D.E.W. Vaughan, H. Thomann, Characterization of iron in zeolites by X-band and Q-band ESR, pulsed ESR, and UV–visible spectroscopies. *J. Am. Chem. Soc.* **116**(14), 6344–6353 (1994). <https://doi.org/10.1021/ja00093a039>
21. A.A. Jahagirdar, N. Dhananjaya, D.L. Monika, C.R. Kesavulu, H. Nagabhushana, S.C. Sharma, B.M. Nagabhushana, C. Shivakumara, J.L. Rao, R.P.S. Chakradhar, Structural, EPR, optical and magnetic properties of $\alpha\text{-Fe}_2\text{O}_3$ nanoparticles. *Acta Part A Mol. Biomol. Spectrosc.* **104**, 512–518 (2013). <https://doi.org/10.1016/j.saa.2012.09.069>
22. C.L. Benyacko, G.T. Hauser, R.J. Rawson, A.J. Sherman, Q.L. Wiebe, K. Poottafai, D.R. Talham, M.W. Meisel, Cryogel and Pyrogel magnetism data—2025. OSF (2025). <https://doi.org/10.17605/OSF.IO/GBPUY>, <https://osf.io/gbpuy>

Publisher's Note Springer Nature remains neutral with regard to jurisdictional claims in published maps and institutional affiliations.

Springer Nature or its licensor (e.g. a society or other partner) holds exclusive rights to this article under a publishing agreement with the author(s) or other rightsholder(s); author self-archiving of the accepted manuscript version of this article is solely governed by the terms of such publishing agreement and applicable law.

Authors and Affiliations

Caeli L. Benyacko^{1,5}  · Garrett T. Hauser^{1,6} · Raven J. Rawson¹ · Alan J. Sherman¹ · Quinton L. Wiebe¹ · Krittin Poottafai³ · Daniel R. Talham³  · Mark W. Meisel^{1,2,4} 

✉ Daniel R. Talham
talham@chem.ufl

✉ Mark W. Meisel
meisel@phys.ufl.edu

Caeli L. Benyacko
benyacko@ucsb.edu

Garrett T. Hauser
Garrett.Hauser@colorado.edu

Raven J. Rawson
rr.jewel00@gmail.com

Alan J. Sherman
alanshermancas@gmail.com

Quinton L. Wiebe
quinton@qleeholdings.com

Krittin Poottafai
krittinpoottafai@ufl.edu

- ¹ Department of Physics, University of Florida, 2001 Museum Road, Gainesville, FL 32611-8440, USA
- ² MagLab High B/T Facility, University of Florida, 2001 Museum Road, Gainesville, FL 32611-8440, USA
- ³ Department of Chemistry, University of Florida, 165 Buckman Drive, Gainesville, FL 32611-7200, USA
- ⁴ Institute of Physics, Faculty of Science, P. J. Šafárik University, Park Angelinum 9, 040 01 Košice, Slovakia
- ⁵ Present Address: Materials Department, University of California, Santa Barbara, CA 93106-5050, USA
- ⁶ Present Address: Department of Applied Mathematics, University of Colorado, Boulder, CO 80309-0526, USA